Constructing the Universe with Clusters of Galaxies, IAP 2000 meeting, Paris (France) July 2000
Florence Durret & Daniel Gerbal eds.

PHYSICAL PROPERTIES OF ABELL 85 INTRA-CLUSTER MEDIUM

G.B. LIMA NETO[1], V. PISLAR[2], J. BAGCHI[3]
[1] *Instituto Astronômico e Geofísico – Universidade de São Paulo, Av. Miguel Stefano 4200, 04301-904 São Paulo/S.P., Brazil*
[2] *Université du Havre, 25, rue Philippe Lebon, F-76600 Le Havre, France*
[3] *Inter-University Centre for Astronomy & Astrophysics, Post Bag 4, Ganeshkhind, Pune 411007, India*

The Intra Cluster Medium is supposed to have been enriched by metal rich, strong galactic wind that develops early in the galaxy history. Through the analysis of BeppoSAX data of Abell 85, in the [0.15-10] keV range, we were able to obtain a low spatial resolution maps of temperature, abundance (basicly iron) and nH. We also derive alpha-elements/iron abundance ratios for the whole cluster and the central region. We obtain values higher than 1 in solar units. These results tend to support the burst model for elliptical galaxies, where type II SN may have the main role in the enrichment of the ICM. We also give new estimates of the magnetic field in Abell 85.

1 Introduction

The hot ($T \approx 10^8$K; central density, $n_0 \approx 10^{-3}$cm^{-3}) X-ray emitting gas found in rich clusters of galaxies is an excellent tool to probe the cluster dynamics, morphology, and history.

The intra-cluster gas accounts for $\sim$ 10–15 % of the total cluster mass and thanks to its short relaxation time scale, it can track the cluster global gravitational potential. The main emission mechanism is the thermal bremsstrahlung that is proportional to $\sim n^2 T^{1/2}$.

The radio observation of diffuse synchrotron radiation strongly suggests the presence of a large scale magnetic field, B, and relativistic electrons in clusters of galaxies.

2 The Data

Abell 85 was observed in July 1998 by the BeppoSAX satellite by two of the narrow field instruments: the LECS, sensitive in the [0.1–10.0] keV range, and the MECS 2 and 3, sensitive in the [1.3–10.5] keV range. The observation was not pointed at the centre of the cluster but at the position of the VSSRS 0038-096. The net exposure time was 92 708 and 40 810 s for the MECS and LECS, respectively.

We have defined sub-regions in the field of view in order to perform separate spectral analysis. The X-ray data in these regions were extracted with XSELECT 1.4. Table 1 resumes the characteristics of the regions we have used. Figure 1 shows these sub-regions.

Table 1: Regions used in the spatial/spectral analysis of Abell 85. The fluxes and luminosities are estimated using an absorbed MEKAL model.

Name	Count rate (counts/s)	Flux* [2–10] keV	L_X† [2–10] keV	Localisation
Centre	0.259 ± 0.002	4.37	6.13	Circle at $0^h41^m50^s.27$, $-9°18'12.0''$, radius $1.9'$.
South Blob	0.091 ± 0.001	1.53	2.13	Circle at $0^h41^m44^s.33$, $-9°23'52.0''$, radius $3.2'$.
VSSRS	0.0331 ± 0.0006	0.55	0.77	Circle at $0^h41^m30^s.27$, $-9°22'56.0''$, radius $2.3'$.
North VSSRS	0.0362 ± 0.0007	0.61	0.85	Circle at $0^h41^m20^s.95$, $-9°18'04.0''$, radius $2.9'$.
1st Ring	0.220 ± 0.002	3.70	5.18	Ring between $2.0'$ and $4.7'$, centred at $0^h41^m50^s.27$, $-9°18'12.0''$. The region outside $8'$ from the MECS axis is excluded.
2nd Ring	0.111 ± 0.001	1.86	2.60	Ring between $4.7'$ and $9.4'$, centred at $0^h41^m50^s.27$, $-9°18'12.0''$. The region outside $8'$ from the MECS axis is excluded.
3rd Ring	0.01176 ± 0.0005	1.98	0.17	Region outside the circle centred at $0^h41^m50^s.27$, $-9°18'12.0''$ and radius $9.4'$, excluding the region outside $8'$ from the MECS axis.
All Field	0.587 ± 0.003	9.95	13.94	Circle at $0^h41^m30^s.27$, $-9°22'56.0''$ radius $8.0'$.

* Flux is in units of 10^{-11}erg s^{-1} cm^{-2}
† Luminosity is in units of 10^{44} erg s^{-1}

For each region we have used a single temperature plasma, the MEKAL (Kaastra & Mewe 1993; Liedahl et al. 1995) model. For some regions (centre, South Blob and VSSRS) we have also modelled the intracluster medium with a combination of two models: either two MEKAL or a MEKAL plus a power-law, this to take into account the non-thermal emission. When the counts were high enough, we also have tried the VMEKAL model, i.e., with variable individual abundances rates for the elements. The spectral fits were done using XSPEC v10.0.

3 Estimation of Magnetic Fields

We have attempted to separate the thermal and non-thermal X-ray emission components in two regions where radio observations have detected steep spectrum, diffuse synchrotron radiation – the VSSRS and the South Blob. We estimate the volume averaged magnetic field strengths in these zones, assuming that the detected non-thermal X-ray radiation is due to inverse Compton scattering on the redshifted 2.7 K CMBR photons.

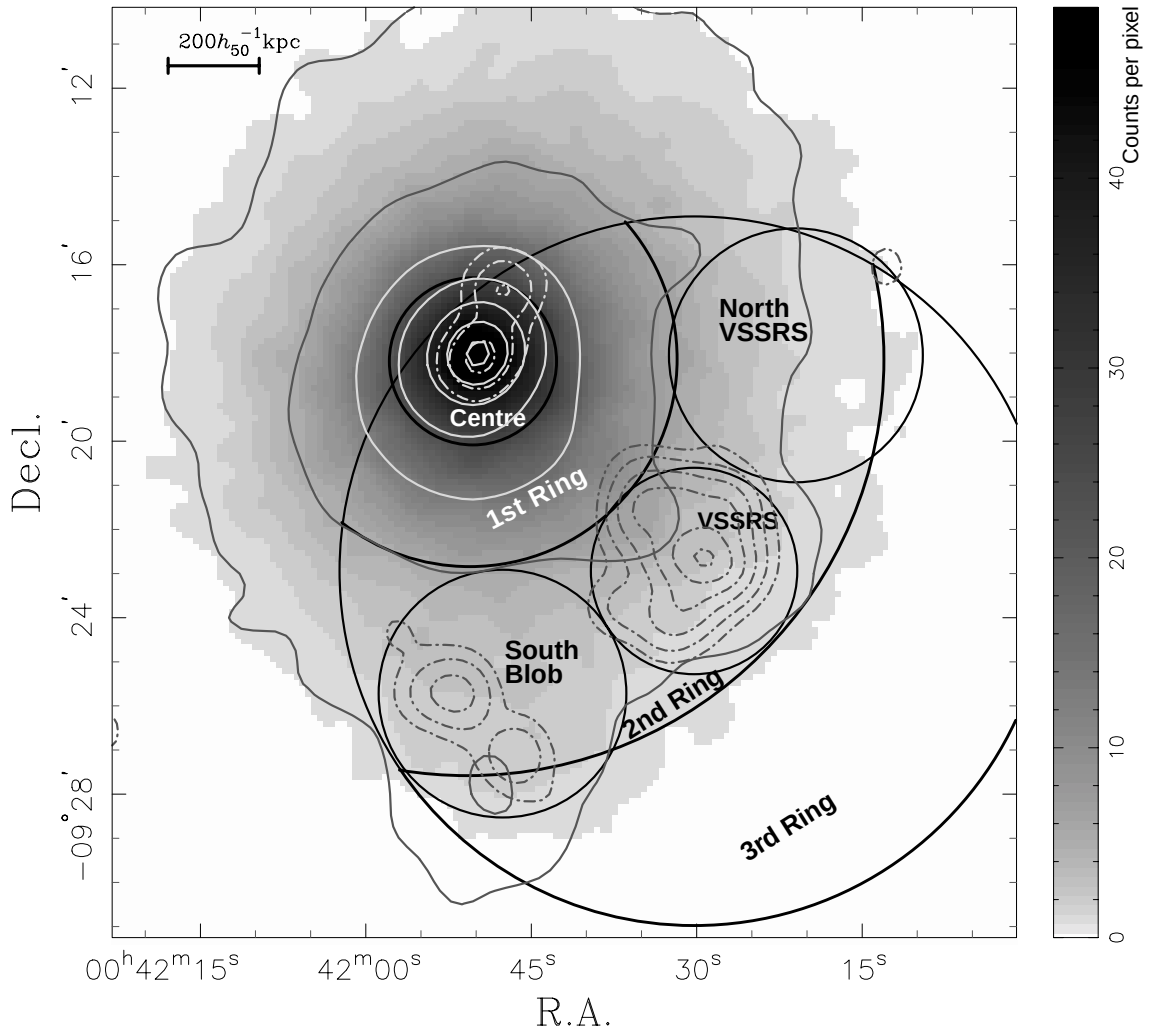

Figure 1: The regions used for the analysis of MECS and LECS data of Abell 85 are the black circles and rings. In grey-scale is the MECS23 image. The continuous gray (white in the centre for the sake of visibility) lines are contours of the PSPC data smoothed with a $\sigma = 0.45$ arcmin Gaussian. The dot-dashed lines are contours from the VLA radio continuum map at 90 cm λ (see text).

3.1 The VSSRS region

When the spectral indices of non-thermal X-ray and radio photons are both fixed at $\alpha_1 = 1$, the IC/3K flux ($f_{\rm IC}$) is estimated to be 3.3×10^{-13}erg s^{-1}cm^{-2} in 2–10 keV range and the radio flux ($f_{\rm S}$) to be 6.6×10^{-14}erg s^{-1}cm^{-2} in 10–100 MHz range. This leads to a field value of $B = 1.34 \pm 0.24 \mu$G.

When we have allowed the spectral index to vary, we have obtained the value of $\alpha_1 = 0.4$, with large error bars (Table 2). This value of spectral index seems roughly consistent with radio spectral shape in the range 10–45 MHz (Bagchi, Pislar & Lima Neto 1998). In this case we have $f_{\rm IC} = 1.2 \times 10^{-12}$erg s^{-1}cm^{-2} and $f_{\rm S} = 4.4 \times 10^{-14}$erg s^{-1}cm^{-2}. From these, we then obtain $B = 0.40 \pm 0.13 \mu$G.

Thus, we have $B = 0.92 \pm 0.35 \mu$G, consistent with our earlier value using ROSAT data (Bagchi et al. 1998).

Table 2: 2-component gas model results. The Flux is without absorption in units of 10^{-11}erg s^{-1} cm^{-2}, where Flux$_1$ and Flux$_2$ refer either to the thermal and non-thermal component, respectively, or to two thermal components (in the MEKAL+MEKAL case). '2POW' means broken power-law.

Region	Models	N_H (10^{20}cm^{-2})	T_1 (keV)	Z_1 ($Z_\odot$)	T_2 (keV)	Z_2 ($Z_\odot$)	α	Flux$_1$ [2–10] keV	Flux$_2$ [2–10] keV	χ^2/dof
Centre	MEKAL+MEKAL	$5.5^{\dagger}$	$6.6^{\dagger}$	$0.38^{\dagger}$	$5.9^{+3.7}_{-2.0}$	$1.0^{\dagger}$	—	3.55	0.86	228.41/162
Centre	MEKAL+MEKAL	$9.5^{+3.8}_{-2.7}$	$6.6^{\dagger}$	$0.38^{\dagger}$	$6.1^{+5.5}_{-3.8}$	> 0.4	—	0.52	3.89	198.98/160
Centre	MEKAL+MEKAL	$11.8^{+3.4}_{-2.9}$	$6.0^{+0.4}_{-0.4}$	$0.48^{+0.10}_{-0.09}$	$2.2^{+6.7}_{-1.3}10^{-2}$	> 0.0	—	4.42	0.00	178.70/158
Centre	MEKAL+POW	$9.4^{+4.5}_{-2.6}$	$6.2^{+0.5}_{-0.4}$	$0.48^{+0.10}_{-0.09}$	—	—	$1.0^{\dagger}$	4.42	0.00	198.93/160
S. Blob	MEKAL+POW	$5.3^{+8.1}_{-1.9}$	$7.1^{+1.7}_{-3.1}$	$0.25^{+0.20}_{-0.16}$	—	—	$1.3^{+1.7}_{-1.3}$ *	1.47	0.064	127.05/106
VSSRS	MEKAL+POW	$3.8^{+5.2}_{-1.8}$	$6.7^{+2.8}_{-1.4}$	$0.33^{+0.59}_{-0.27}$	—	—	$1.0^{\dagger}$	0.52	0.033	104.37/107
VSSRS	MEKAL+POW	$3.5^{+5.7}_{-1.5}$	$5.5^{+4.3}_{-2.6}$	$0.35^{+1.59}_{-0.29}$	—	—	$0.4^{+4.8}_{-0.4}$	0.44	0.12	104.04/106
		N_H (10^{20}cm^{-2})	T_1 (keV)	Z_1 ($Z_\odot$)	α_1	Break (keV)	α_2	Flux$_1$ [2–10] keV	Flux$_2$ [2–10] keV	χ^2/dof
VSSRS	MEKAL+2POW	$4.0^{+1.9}_{-1.5}$	$7.3^{+2.7}_{-1.4}$	$0.34^{+0.23}_{-0.17}$	$1.0^{\dagger}$	> 0	$1.85^{\dagger}$	0.52	0.03	103.71/106
VSSRS	MEKAL+2POW	$3.7^{+1.5}_{-1.0}$	$3.9^{+5.7}_{-1.4}$	$0.44^{+0.43}_{-0.25}$	$0.4^{\dagger}$	$7.4^{+0.9}_{-0.7}$ *	$1.85^{\dagger}$	0.27	0.28	101.22/106

* 1σ error

† Value fixed

3.2 The 'South Blob' region

The spectral index value for the emission from the South Blob is not available. However, the radio data from Ooty Synthesis Telescope at 327 MHz detects the total 450 mJy diffuse radio flux from this zone (Bagchi et al. 1998). By model fitting, we have obtained an estimate of 6.4×10^{-13}erg s^{-1}cm^{-2} for the IC/3K flux and $\alpha = 1.3$ for the spectral index. Assuming this as the radio spectral index, we can calculate the value for magnetic field, $B = 0.42 \pm 0.20\mu$G.

4 Metallicity

The mean value obtained for the whole cluster is $0.38 \pm 0.06 Z_\odot$ (3σ error), i.e., the usual value found in clusters with the same temperature of Abell 85 and very close to the one found by Pislar et al. (1997).

For the individual iron abundance, we systematically obtain a lower value compared to the mean abundance of all metals. The mean value for the whole field is 0.30 ± 0.05 (3σ error).

The individual abundances of other metals (except perhaps for Ni) obtained with the VMEKAL model are usually higher than the iron abundance (Table 4). The ratio of α-elements (Si, S, Ar and Ca) to iron is greater than one (in solar units). However, the Ni/Fe abundance ratio is systematically lower than the α-elements/Fe.

Our result supports the burst model for elliptical galaxies, where a strong galactic wind develops early in the galaxy history (Martinelli et al. 1999). The burst model predicts an overabundance of α-elements compared to Fe. The bi-modal model proposed by Elbaz et al. (1995) also predicts a higher abundance of Si compared to Fe. Following their conclusion, our results suggest that type II SN have the main role in the enrichment of the ICM. Fukazawa et al. (1998) also suggests that, if the Si/Fe relative abundance is indeed correlated with the cluster temperature, then the role of type II SN should be more important for hotter clusters.

5 Cooling-flow

We find a lower temperature in the central region, compared to the mean cluster temperature. The difference in temperature we find is only ≈ 0.5 keV, and, given our 3σ error bars, this is

Table 3: Abundances relative to iron for all field, the centre region and the first two rings. The numbers in brackets give the observed 1σ interval.

	Si	S	Ar	Ca	Ni
all field	2.0	0.7	1.0	2.0	0.3
	[3.0–1.0]	[1.7–0.0]	[3.0–0.0]	[4.0–0.0]	[1.7–0.0]
Centre	1.8	1.5	2.5	6.0	1.0
	[2.8–0.8]	[2.8–0.5]	[4.8–0.5]	[8.2–4.0]	[2.5–0.0]
1st Ring	2.1	—	3.6	—	0.4
	[3.6–0.7]	—	[6.8–0.4]	—	[2.5–0.0]
2nd Ring	4.7	2.9	—	3.5	4.7
	[8.2–1.1]	[6.5–0.0]	—	[11.1–0.0]	[10.0–0.0]

also compatible with an isothermal temperature profile. However, at 1σ level, the temperature is not isothermal.

We have a better fit using a 2-temperature plasma model, with one of the components being very cold, Fig. 2. This cold component could be related to the Extreme Ultra-Violet (EUV) excess observed in some clusters by the EUVE satellite (Lieu et al. 1996; Lieu et al. 1999).

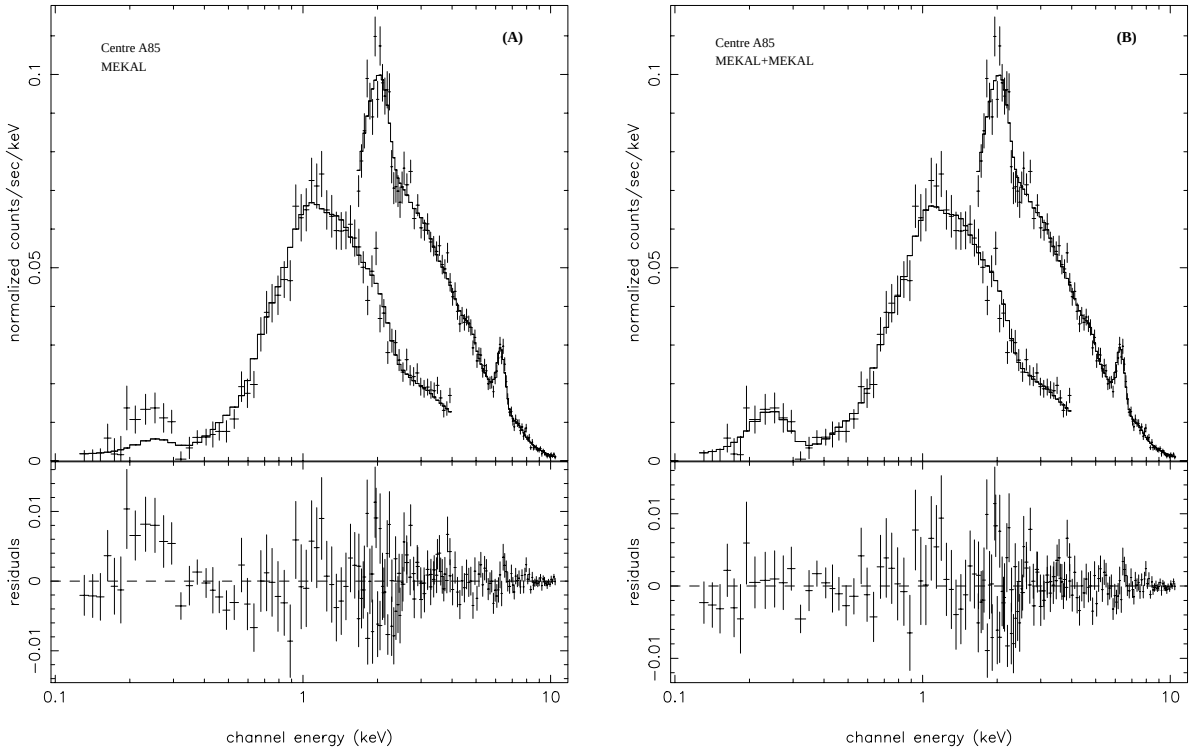

Figure 2: Plasma model fits to the centre region of Abell 85. Left: Single temperature MEKAL model. Right: two temperature model. Notice the low energy photon excess in panel (A) compared to the two temperature model (B).

6 Cluster merging at the South Blob

The temperature detected in the South Blob is higher than in the other regions of Abell 85 [c.f. also Markevitch et al. (1998) using ASCA data]. This may be interpreted by Durret et al. (1998)

model, i.e., of a substructure falling in the main body of Abell 85. The higher temperature may be explained by a shock that heats the ICM.

The South Blob presents a significantly lower abundance of metals compared to the other regions of Abell 85. If we admit that a filament of very low surface brightness is falling into Abell 85, along the axis coming from Abell 87 (composed by poor sub-clusters), then we can suppose that the gas has a rather low metallicity. This could explain the low abundance at the South Blob as the mixture of the $Z \sim 0.4 Z_{\odot}$ ICM from Abell 85 with a poor-metal gas falling along the filament.

If the South Blob is indeed a place where a substructure is merging with the main body of Abell 85, then we may have a strong shock in this region. Such a shock is bound to accelerate the ICM electrons to relativistic energies (Enßlin et al. 1998; Sarazin 1999) and thus produce X-ray emission. Although the relativistic electrons are there, since we can observe diffuse synchrotron radio emission at 328 and 1400 Mhz in this region, we could not unambiguously detect the X-ray IC emission.

7 Conclusion

Our results are summarized below and in Fig. 3:

- We have derived an abundance ratio between α-elements/iron greater than 1 and the iron metallicity is systematically lower than the mean metallicity. The over abundance of α-elements may be an indication of an early enrichment of the ICM by type II supernovae in elliptical galaxies.
- The central region is better fitted with two temperature components, the lower temperature being lower than ~ 0.1 keV. This supports the existence of a central cooling-flow.
- Although we could not separate unambiguously the thermal from the non-thermal X-ray emission, we have estimated, with different fitting procedures, the non-thermal X-ray flux. From these values and the radio spectrum data we derive the intensity of the extended magnetic field to be $B = 0.92 \pm 0.35 \mu$G.
- The South-Blob region shows a significantly lower metallicity than the rest of the cluster. Its temperature is also higher than its neighbouring regions. Such results support the picture of a falling stream merging with the main body of Abell 85 in that region.

Acknowledgments

GBLN acknowledge the USP/COFECUB cooperation and the FAPESP (*Fundação de Amparo à Pesquisa do Estado de São Paulo*).

References

1. Bagchi J., Pislar V., Lima Neto G.B., 1998, MNRAS 296, L23
2. Boella G., Butler R.C., Perola G.C., Piro L., Scarsi L., Bleeker J.A.M., 1997a, A&AS 122, 299
3. Boella G., Chiappetti L., Conti G., Cusumano G., del Sordo S., La Rosa G., Maccarone M.C., Mineo T., Molendi S., Re S., Sacco B., Tripiciano M., 1997b, A&AS 122, 327
4. Durret F., Forman W., Gerbal D., Jones C., Vikhlinin A., 1998, A&A 335, 41
5. Elbaz D., Arnaud M., Vangioni-Flam E., 1995, A&A 303, 345
6. Enßlin T.A., Biermann P.L., Klein I., Kohle S., 1998, A&A 332, 395

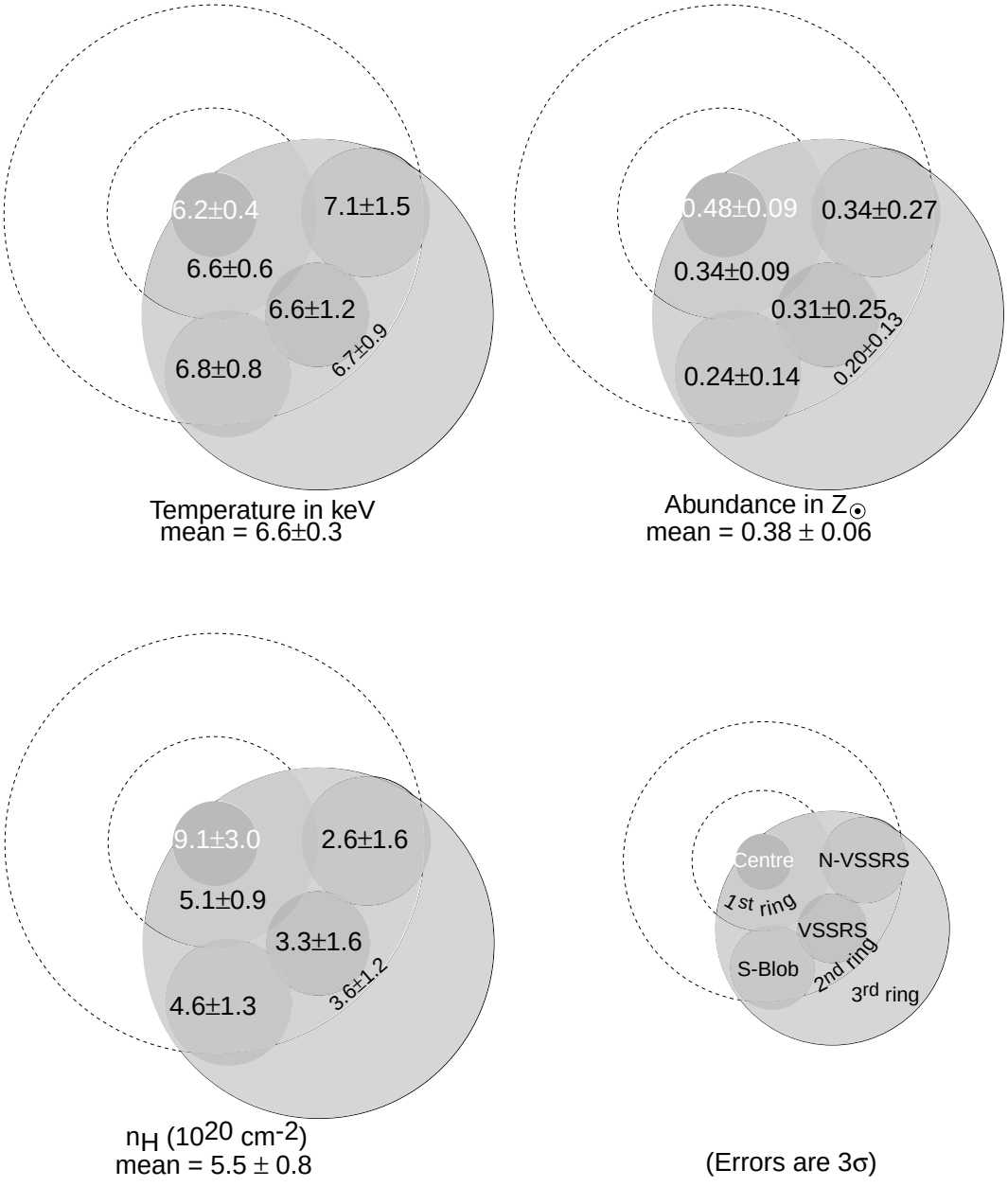

Figure 3: Spatial distribution of the temperature, metallicity and hydrogen column density.

7. Feretti L., Giovannini G., 1996, IAU Symp. 175 "Extragalactic Radio Sources", p. 333 (Ekers R., et al. eds.) Kluwer: Dordrecht
8. Fukazawa Y., Makishima K., Tamura T., Ezawa H., Haiguang X., Ikebe Y., Kikuchi K., Ohashi T., 1998, PASJ 50, 187
9. Kaastra J.S., Mewe R., 1993, A&AS 97, 443
10. Liedahl D.A., Osterheld A.L., Goldstein W.H., 1995, ApJ 438, L115
11. Lieu R., Mittaz J.P.D., Bowyer S., Breen J.O., Lockman F.J., Murphy E.M., Hwang C.Y., 1996, Science 274, 1335
12. Lieu R., Bonamente M., Mittaz J.P.D., Durret F., Dos Santos S., Kaastra J., 1999, ApJ 527, L77
13. Lima Neto G.B., Pislar V., Durret F., Gerbal D., Slezak E., 1997, A&A 327, 81
14. Loewenstein M., Mushotzky R.F.,1996, ApJ 466, 695
15. Markevich M., Forman W.R., Sarazin C.L., Vikhlinin A., 1998, ApJ 503, 77
16. Martinelli A., Matteucci F., Colafrancesco S., 2000, A&A 354, 387
17. Mushotzky R.F., Loewenstein M., Arnaud K.A., Tamura T., Fukazawa Y., Matsushita K., Kikuchi K., Hatsukade I., 1996, ApJ 466, 686
18. Pislar V., Durret F., Gerbal D., Lima Neto G.B., Slezak E., 1997, A&A 322, 53
19. Sarazin C.L., 1999, ApJ 520, 529